Research Article | Vol. 27, No. 15 | 22 Jul 2019 | OPTICS EXPRESS 20479
Optics EXPRESS

Versatile and precise quantum state engineering by using nonlinear interferometers

JIE SU,[1,3] LIANG CUI,[1,3] JIAMIN LI,[1] YUHONG LIU,[1] XIAOYING LI,[1,*] AND Z. Y. OU[1,2,4]

[1] *College of Precision Instrument and Opto-Electronics Engineering, Key Laboratory of Opto-Electronics Information Technology, Ministry of Education, Tianjin University, Tianjin 300072, China*
[2] *Department of Physics, Indiana University-Purdue University Indianapolis, Indianapolis, IN 46202, USA*
[3] *These authors contributed equally to this work.*
[4] *zheyuou@tju.edu.cn*
[*] *xiaoyingli@tju.edu.cn*

Abstract: The availability of photon states with well-defined temporal modes is crucial for photonic quantum technologies. Ever since the inception of generating photonic quantum states through pulse pumped spontaneous parametric processes, many exquisite efforts have been put on improving the modal purity of the photon states to achieve single-mode operation. However, because the nonlinear interaction and linear dispersion are often mixed in parametric processes, limited successes have been achieved so far only at some specific wavelengths with sophisticated design. In this paper, we resort to a different approach by exploiting an active filtering mechanism originated from interference fringe of nonlinear interferometer. The nonlinear interferometer is realized in a sequential array of nonlinear medium, with a gap in between made of a linear dispersive medium, in which the precise modal control is realized without influencing the phase matching of the parametric process. As a proof-of-principle demonstration of the capability, we present a photon pairs source using a two-stage nonlinear interferometer formed by two identical nonlinear fibers with a standard single mode fiber in between. The results show that spectrally correlated two-photon state via four wave mixing in a single piece nonlinear fiber is modified into factorable state and heralded single-photons with high modal purity and high heralding efficiency are achievable. This novel quantum interferometric method, which can improve the quality of the photon states in almost all the aspects such as modal purity, heralding efficiency, and flexibility in wavelength selection, is proved to be effective and easy to realize.

1. Introduction

High quality photonic quantum states are essential resource for fundamental test of quantum mechanics and for quantum information [1–4]. Although recent advances in quantum computers put focus on trapped ions and superconducting qubits because of their ability to scale up [5,6], optical qubits are nevertheless still quite popular ever since the beginning of the quantum information processing (QIP) [3]. This is mostly because of the easiness in generation and manipulation of photons. Moreover, quantum communication in a quantum network highly relies on photons as information carrier [4,7]. Recently, quantum simulations such as Boson sampling are also achieved with photonic states [8,9]. On the other hand, optical QIP protocols, such as quantum teleportation and entanglement swapping etc., rely on quantum interference of photons for the desired results [3,4,7–11]. Nowadays, despite of the tremendous advances in the on-demand generation of single photons [12,13], the most economic and convenient photon sources are from spontaneous parametric processes, in the form of either two-photon states or heralded single-photons by projecting on the detection of one of the two-photons [14]. So, if more than two photons are involved in optical QIP, the photons are most likely from two or more independent sources of spontaneous parametric processes [7–11].

#364965 https://doi.org/10.1364/OE.27.020479
Journal © 2019 Received 12 Apr 2019; revised 13 Jun 2019; accepted 14 Jun 2019; published 9 Jul 2019

Optics EXPRESS

Quantum interference stems from indistinguishability, which requires the mode match between photons. On the other hand, because of the broadband nature of spontaneous parametric processes using pulsed lasers as the pump, frequency or temporal correlation of two-photon states are usually very complicated. As a result, the photons generated from these processes are of multi-mode nature [15, 16]. This diminishes quantum interference effects and thus prevents optical QIP protocols from achieving desired goals. There are two approaches for combating the temporal indistinguishability issue: one is to use a narrow band two-photon source so that photo-detectors are fast enough to resolve the arrival of photons [17]; the other is to engineer the spectrum of spontaneous parametric processes to achieve single mode operation [11, 15, 16, 18]. The latter approach is more popular because of the easiness in operation and the precise timing in pulsed mode.

For the pulsed operation, the foremost issue is the temporal profile of pulses. Since the temporal mode and spectral mode of an optical field are Fourier transform of each other, in this paper, we use the term temporal modes to describe the temporal-spectral property of photon states. It was realized in the early days that a factorized joint spectral function (JSF) of the two-photon state is required for the single mode operation [15, 19]. A straightforward method to obtain factorable JSF is reshaping the spectrum with optical filters [7, 20]. However, passive filtering usually deletes photons at random, thus destroying two-photon correlation and resulting in low two-photon events [21]. This detrimental effect of passive optical filters leads to the idea of spectral engineering parametric processes to achieve factorization without filtering [15, 16]. Tremendous efforts were spent through the years along this line, including the employment of photonic grating for active temporal mode shaping [22], special selection of $\chi^{(2)}$-nonlinear crystals with desired properties [18], engineering of the dispersion of nonlinear optical fibers [23–27], and engineering of the structure of nonlinear photonic crystals [28, 29]. While most sources were successful to some extent, many are limited to a specific wavelength range of operation due to strict requirement on dispersion and phase matching. The operation ranges of these sources are usually restricted to tens of nanometers, and a tunable pump is usually required to achieve this kind of tunability.

The JSF of spontaneous parametric processes is affected by dispersion-dependent phase-matching condition. Thus, changing dispersion will affect the phase matching, leading to complicated dependence of JSF on dispersion. So everything has to be perfect to achieve the goals. This is why most of the schemes are lack of tunability. In this paper, we resort to a different approach in which we separate nonlinear gain control from linear dispersion engineering by the method of controlling quantum interference in nonlinear interferometer [30–32]. The nonlinear interferometer (NLI), originally designed to achieve the Heisenberg limit in precision phase measurement [33], has found applications in quantum interferometry beyond standard quantum limit [34], in imaging with undetected photons [35], and in infrared spectroscopy [36], etc. Here we investigate the application of NLI in reshaping the JSF. Different from previous NLIs containing two pieces of nonlinear media [36], our NLI is realized in a sequential array of nonlinear media, with a gap in between made of a linear dispersive medium, in which the precise modal control is realized without influencing the phase matching of the parametric process. Moreover, we will extend NLI from two-stage to multi-stage, in which the number of nonlinear media is greater than two.

Figure 1 shows the conceptual representation of the nonlinear interferometer. The pulse-pumped nonlinear interferometer achieves quantum interference between two nonlinear interaction processes taken place in nonlinear media (NMs) NM_1 and NM_2, respectively, so that the outcome depends on the phases in between. We can therefore realize spectral control and shaping with a linear dispersive medium (DM) independent of the nonlinear interaction processes. Using the interferometric method, we are able to engineer the JSF of photon pairs at the output of NLI. Indeed, an NLI formed by two pieces of $\chi^{(2)}$-nonlinear crystals with a quartz spacer in

Optics EXPRESS

between had been used to experimentally modify the spectral correlation of a two-photon state from asymmetry to symmetry [37]. Here we will show that the NLI can improve the quality of the photon states in almost all the aspects such as modal purity, heralding efficiency, brightness and wavelength tunability.

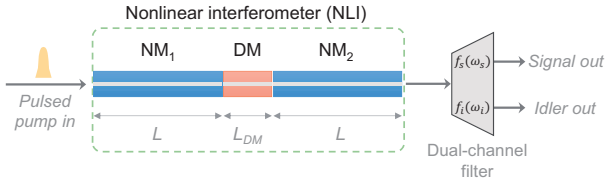

Fig. 1. Conceptual representation of the SU(1,1)-type nonlinear interferometer (NLI) consisting of two identical nonlinear media (NM_1 and NM_2) with a linear dispersive medium (DM) in between. $f_s(\omega_s)$ and $f_i(\omega_i)$ are the transmission functions for signal and idler output fields provided by dual-channel filter.

The rest of the paper is organized as follows. Base on the theoretical model in Fig. 1, in Sect. 2, we first examine the output characteristics of a two-stage NLI and compare it with that of a single piece NM through a series of simulations. To avoid the complexity originated from the coupling between spatial and temporal modes of photon pairs [21], we assume that the NMs are in waveguide structure and support single spatial mode. In Sect. 3 we verify the theoretical analysis by performing an experiment using a two-stage NLI, which is formed by two identical single mode nonlinear fibers with a standard single mode fiber in between. The experimental data agrees with the theoretical predictions. However, the results indicate that the temporal mode property of photon pairs obtained from two-stage NLI slightly deviates from the ideal case of single mode. We then discuss how to better control the temporal mode of photon pairs by extending the theory of the two-stage NLI to the multi-stage NLI in Sect. 4. Finally, we briefly conclude in Sect. 5.

2. Theoretical analysis and simulation results

Since single photons and single photon qubits are among the foundations of most quantum optical information processing technique, let's start from analyzing the modal purity of single photon state. Single-photon state can be obtained by heralding on the detection of one of the two-photons. It can be shown that the purity of the heralded single-photon state with density operator $\hat{\rho}_1$ has the following form [32]:

$$p = \mathrm{Tr}(\hat{\rho}_1^2) = h^2/K + (1-h)^2, \tag{1}$$

where $K \geq 1$ is Schmidt mode number [38] and $h \leq 1$ is heralding efficiency [32] after excluding the detection efficiencies of the two-photons. The definition of h is given later in Eq. (6), which shows the heralding efficiency usually depends on the spectra of the two-photons and the filters applied. Ideally, we prefer to have $p = 1$ for $K = 1$ and $h = 1$.

In general, the quantum state from spontaneous parametric process has the form of [19]

$$|\Psi\rangle \approx |vac\rangle + G|\Psi_2\rangle \tag{2}$$

with the two-photon state

$$|\Psi_2\rangle = \int d\omega_s d\omega_i F(\omega_s, \omega_i)\hat{a}_s^\dagger(\omega_s)\hat{a}_i^\dagger(\omega_i)|vac\rangle, \tag{3}$$

where $|vac\rangle$ represents the vacuum state, $F(\omega_s, \omega_i)$ is the joint spectral function (JSF) for the generated two photons dubbed "signal" and "idler" with $\omega_{s,i}$ denoting their frequencies, and G is a quantity related to the power of the pump.

Schmidt mode number K is related to the normalized intensity correlation function [19]

$$\bar{g}^{(2)} = 1 + 1/K = 1 + \mathcal{E}/\mathcal{A}, \tag{4}$$

with $\bar{g}^{(2)} = 2$ or $K = 1$ for single mode case and

$$\begin{aligned} \mathcal{E} &\equiv \int d\omega_s d\omega_i d\omega_s' d\omega_i' \bar{F}(\omega_s, \omega_i)\bar{F}(\omega_s', \omega_i') \\ &\quad \times \bar{F}^*(\omega_s, \omega_i')\bar{F}^*(\omega_s', \omega_i), \\ \mathcal{A} &\equiv \int d\omega_s d\omega_i d\omega_s' d\omega_i' |\bar{F}(\omega_s, \omega_i)\bar{F}(\omega_s', \omega_i')|^2, \end{aligned} \tag{5}$$

where $\bar{F}(\omega_s, \omega_i) \equiv F(\omega_s, \omega_i) f_s(\omega_s) f_i(\omega_i)$ is the two-side filtered JSF with $f_{s(i)}(\omega_{s(i)})$ being the transmission function of filter placed in the signal (idler) field. However, the experimentally measurable quantity is the one-side-filtered intensity correlation function $\bar{g}^{(2)}_{s(i)}$ of the individual signal (idler) field, which can be obtained from Eqs. (4)-(5) with $\bar{F}(\omega_s, \omega_i)$ replaced by $F(\omega_s, \omega_i) f_{s(i)}(\omega_{s(i)})$. Generally $\bar{g}^{(2)}_{s(i)}$ sets a lower bound for $\bar{g}^{(2)}$ [32] and we use it for characterizing the modal purity of photon pairs. By definition, the heralding efficiency of the signal (idler) photons is the ratio of probability of recording two-photons, P_c, to that of individual idler (signal) photon, $P_{i(s)}$, and is related to JSF by

$$h_{s(i)} \equiv \frac{P_c}{P_{i(s)}} = \frac{\int d\omega_s d\omega_i |F(\omega_s, \omega_i) f_s(\omega_s) f_i(\omega_i)|^2}{\int d\omega_s d\omega_i |F(\omega_s, \omega_i) f_{i(s)}(\omega_{i(s)})|^2}. \tag{6}$$

Obviously, $h_{s(i)} = 1$ when no filter is applied. Under this condition, it is impossible to obtain $K = 1$ for frequency anti-correlated JSF. With optical filtering, while near unity modal purity ($K \to 1$ or $\bar{g}^{(2)} \to 2$) can be achieved, heralding efficiency drops significantly below one (as demonstrated later in Figs. 2(c) and 2(d)). Moreover, to decrease the contribution of higher photon number states, which degrade the quality of heralded single photons, it is important to make both heralding efficiencies h_s, h_i as high as possible [32, 39].

To investigate the effect of the two-stage NLI in Fig. 1, we employ single-mode dispersion-shifted fibers (DSFs) and conventional standard single-mode fiber (SMF) as the NMs and DM, respectively. We calculate the JSF, modal purity, and heralding efficiency of photon pairs generated from the NLI and compare the results with those obtained from non-NLI case. Here the non-NLI case refers to the situation, in which only one piece of NM of used to generate photon pairs. We first conduct simulation for the non-NLI case of a single-piece DSF. For the photon pairs from pulse-pumped spontaneous four-wave mixing (SFWM) process in a DSF with length L, the JSF is written as [40]

$$\begin{aligned} F_{NM}(\omega_s, \omega_i) &\propto \exp\left[-(\omega_s + \omega_i - 2\omega_{p0})^2(1 + jC_p)/4\sigma_p^2 \right] \\ &\quad \times \mathrm{sinc}(\Delta k L/2) e^{j(\Delta k L/2)} \end{aligned} \tag{7}$$

where ω_{p0}, σ_p and C_p are the central frequency, spectral width and chirp of pump, respectively, $\Delta k = 2k(\omega_p) - k(\omega_s) - k(\omega_i) - 2\gamma P_p$ with γ and P_p respectively denoting the nonlinear coefficient and peak pump power is the wave vector mismatch between the pump, signal, and idler fields in DSF. Using Eq. (7), we plot in Fig. 2(a) the JSF ($|F_{NM}(\omega_s, \omega_i)|^2$) from a single-piece 600-m-long DSF. We also calculate the marginal intensity distribution for the signal (idler) field ($\int d\omega_{i(s)} |F_{NM}(\omega_s, \omega_i)|^2$). Owing to the symmetry of the signal and idler fields, we only plot the

Optics EXPRESS

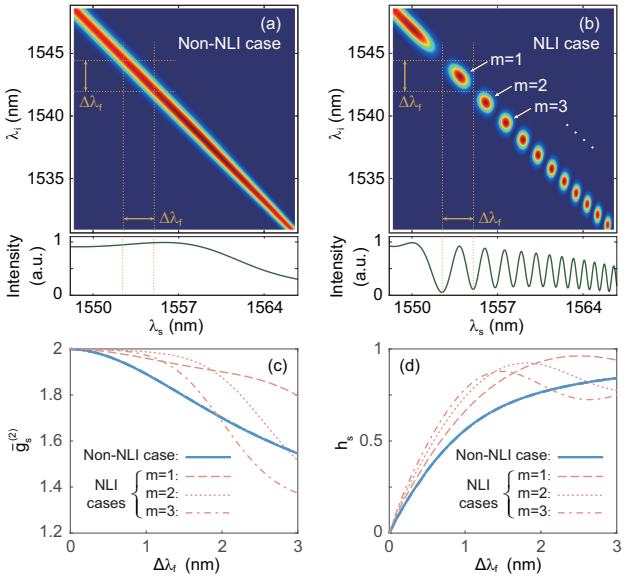

Fig. 2. Contour plots of squared modulus of JSF for (a) the non-NLI case (a 600-m DSF as the single-piece NM) and (b) the NLI case (two 300-m DSFs as the NMs and 17.2-m SMF as the DM). The marginal intensity distributions of signal field are next to the JSFs. Calculated (c) intensity correlation function $\bar{g}_s^{(2)}$ and (d) heralding efficiency h_s as function of filter bandwidth $\Delta\lambda_f$ in signal band for different cases.

calculated results for the signal field in Fig. 2 except for the JSFs. The results are presented in the wavelength space, and the parameters used in our simulation are based on the experiments in Sect. 3, except for the chirp of pump pulses C_p being zero. The JSF in Fig. 2(a) exhibits a strong frequency correlation and thus a low mode purity. To produce a better quality two-photon state, we can respectively apply two filters to the signal and idler fields. Assuming that the central wavelengths of both filters satisfy the energy conservation and have rectangular windows with a common bandwidth of $\Delta\lambda_f$ (in term of wavelength, see the dotted lines in Figs. 2(a) and 2(b)), we calculate the correlation function $\bar{g}_s^{(2)}$ and heralding efficiency h_s of individual signal field using Eqs. (4)-(6) when the detuning between signal/idler and pump fields is about 6 nm. From the results shown in Figs. 2(c) and 2(d) (thick solid curves), one sees $\bar{g}_s^{(2)}$ and h_s have an opposite trend as $\Delta\lambda_f$ changes.

We then examine the NLI case in which a DM (i.e., an SMF) of length L_d is sandwiched between two identical DSFs of length L. Depending on the phase difference induced by DM, two-photon interference occurs between the spontaneous two-photon processes in two DSFs. The JSF is then modified as

$$F_{NLI}(\omega_s, \omega_i) = F_{NM}(\omega_s, \omega_i) e^{j\theta} \cos\theta \tag{8}$$

with

$$\theta \equiv (\Delta k L + \Delta\phi_d)/2, \tag{9}$$

where the phase shift $\Delta\phi_d = \Delta k_d L_d$ induced by DM is wavelength dependent and $\Delta k_d \equiv 2k_d(\omega_p) - k_d(\omega_s) - k_d(\omega_i)$ is the wave vector mismatch between pump and photon pairs per unit length in DM. Equation (8) shows that the interference term $\cos\theta$ determined by dispersion of DM is independent of the nonlinear interaction in each NM described by $F_{NM}(\omega_s, \omega_i)$ in Eq.

7. Usually, we have $\Delta k \rightarrow 0$ to guarantee the satisfaction of phase matching condition in each nonlinear medium. So $\Delta\phi_d$ becomes the main term determining θ, and the interference term $\cos\theta$ in Eq. (8) is mainly determined by dispersion of DM. For the pump, signal and idler fields satisfying the nearly degenerate condition of $|\omega_{s(i)} - \omega_{p0}| \ll \omega_{p0}$, Δk_d can be approximated as $\Delta k_d \approx \frac{1}{4} k_d''(\omega_{p0})(\omega_s - \omega_i)^2$, where $k_d''(\omega_{p0})$ is the second order dispersion of DM at central frequency of pump.

Figure 2(b) shows the simulation result of JSF modified by NLI, in which the lengths of SMF and each DSF are 17.2 and 300 m, respectively. Because of the interference, the modified JSF is divided into islands, which are separated from each other. As a result, the marginal intensities in both the signal and idler fields exhibit similar interference patterns. For brevity, we only plot the marginal intensity in signal field in Fig. 2(b), which is obviously different from the non-NLI case in Fig. 2(a). Due to the interference induced active filtering effect, each island in Fig. 2(b) itself can be viewed as an individual JSF when selected by filters. In this case, the state in Eq. (2) can be written as

$$|\Psi\rangle \approx |vac\rangle + G_m \sum_{m=0} |\Phi_2^{(m)}\rangle, \tag{10}$$

where G_m are properly scaled quantities and $|\Phi_2^{(m)}\rangle$ has the same form as $|\Psi_2\rangle$ in Eq. (3) but with the JSF being changed to $F_{NLI}(\omega_s, \omega_i) f_s^{(m)}(\omega_s) f_i^{(m)}(\omega_i)$. Here, $f_s^{(m)}(\omega_s)$ and $f_i^{(m)}(\omega_i)$ are the rectangular filter functions that can properly isolate the m-th island in the JSF. Taking advantage of the active filtering function of NLI, we expect to simultaneously achieve $h_{s,i} \rightarrow 1$ and $\bar{g}^{(2)}{}_{s,i}$ by properly picking out one island.

For each island, we calculate the correlation function $\bar{g}_s^{(2)}$ of individual signal field using Eqs. (4) and (5) but with $\bar{F}(\omega_s, \omega_i)$ replaced by the modified JSF, $F_{NLI}(\omega_s, \omega_i) f_s^{(m)}(\omega_s)$. Likewise, we evaluate the heralding efficiency h_s from Eq. (6). The results for islands with numbers $m = 1$, 2 and 3 are respectively shown by the dashed, dotted and dash-dot curves in Figs. 2(c) and 2(d). For the sake of comparison, we also conduct simulations for the non-NLI cases when the central wavelengths of photon pairs respectively correspond to the centers of the three islands of NLI. We find that the results of the non-NLI case (thick curves) for photon pairs with different wavelengths cannot be visually identified from each other. Compared with the non-NLI case, one sees that although $\bar{g}_s^{(2)}$ and h_s of the NLI case still behave oppositely as the filter bandwidth $\Delta\lambda_f$ changes, significant improvements can be observed. Especially, there exists an optimum value of $\Delta\lambda_f$ ($\Delta\lambda_f = 2.2$ nm for $m = 1$, 1.5 nm for $m = 2$, and 1.2 nm for $m = 3$), at which h_s reaches its peak (up to 0.9) while $\bar{g}_s^{(2)}$ higher than 1.9 can be maintained. For the idler field, similar improvements can also be observed (not presented in the figure): when the heralding efficiency h_i reaches its peak value of up to 0.9, the correlation function $\bar{g}_i^{(2)}$ maintains higher than 1.9.

Note that the dual-band filter placed at the output of NLI is employed to select out a specific island of JSF. The usage of filter does not significantly alter the spectra of the selected island when the filter bandwidth is optimized, since the spectra-reshaping of NLI is realized by the two-photon quantum interference effect. Therefore, rectangular-shaped filters are preferred in our scheme. In practice, a number of rectangular- or near rectangular-shaped filters with near perfect transmission efficiency are available, such as wavelength-division multiplexing filters and fiber Bragg grating filters. So the filter used in the NLI will not cause the reduction in brightness of photon pairs.

3. Experimental implementation and results

To verify the simulation results in Sect. 2, we experimentally generate photon pairs by using a two-stage NLI. The experimental setup is shown in Fig. 3. The NLI consists of two identical 300-m-long DSFs and a 17.2-m-long standard SMF. The zero group velocity dispersion (GVD)

Optics EXPRESS

wavelength and GVD slope of each DSF with nonlinear coefficient γ of about 2 $(\mathrm{W}\cdot\mathrm{km})^{-1}$ are about 1548.2 nm and 0.075 ps/(km·nm^2), respectively. The GVD coefficient of the SMF is 17 ps/(km·nm) in the vicinity of 1550 nm band. Note that the DSFs serve as NMs, and the standard SMF functions as the linear dispersive medium because the phase matching of SFWM is not satisfied in it. The central wavelength and full width at half maximum (FWHM) of the pulsed pump sent into the NLI are 1548.5 nm and 1 nm, respectively. So the phase matching condition of SFWM is satisfied in DSF. For the photon pairs produced by SFWM in DSF, spontaneous Raman scattering (SRS) is the major source of background noise [41]. We therefore submerge the NLI into liquid nitrogen to suppress SRS. The transmission loss of the NLI is mainly originated from imperfect splicing of DSF and SMF, and transmission efficiency of NLI for all the waves involved in SFWM is about 85 %.

The pulsed pump is obtained from a mode-locked fiber laser, whose central wavelength and repetition rate are about 1550 nm and 41 MHz, respectively. The pulse train from the laser is first filtered by a grating filter (F_1) and amplified by an erbium-doped fiber amplifier (EDFA) to achieve the required power. Then the pulse train is further cleaned up by a Gaussian-shaped bandpass filter F_2 with an FWHM of 1 nm. The pulse duration of the pump is $\sim$ 4.6 ps, corresponding to a linear chirp of $C_p = 0.84$. Note that the existing of chirp will decrease the value of $\bar{g}^{(2)}_{s(i)}$ [26]. The pump power is controlled by a fiber polarization controller (FPC1) and a fiber polarization beam splitter (FPBS1).

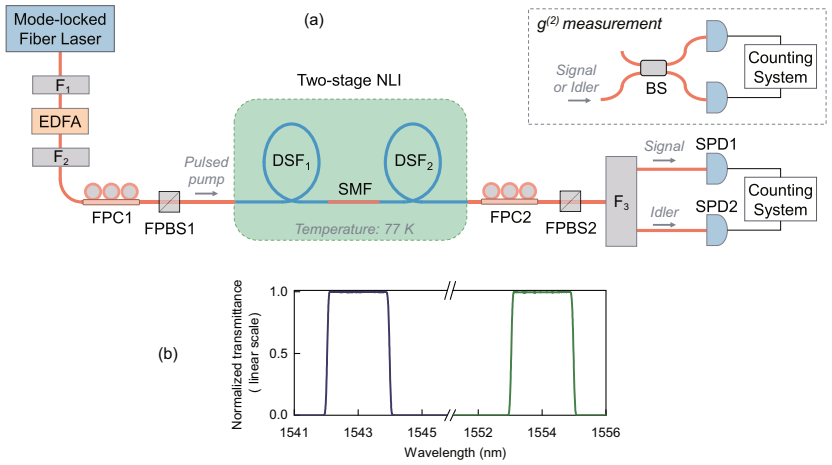

Fig. 3. (a) Experimental setup of generating photon pairs from a two-stage NLI formed by two identical dispersion shifted fibers (DSF) with a standard single mode fiber (SMF) in between. The inset is the setup for measuring intensity correlation function $\bar{g}^{(2)}_{s(i)}$ of individual signal (idler) field. (b) The spectra of dual-band filter F_3. $F_{1(2)}$, single-band filter; EDFA, erbium-doped fiber amplifier; FPC, fiber polarization controller; FPBS, fiber polarization beam splitter; BS, 50/50 beam splitter; SPD, single photon detector.

Because the correlated photon pairs from SFWM are co-polarized with the pump while the noise photons from SRS are scattered to all polarization directions, FPC2 and FPBS2 at the output port of the NLI are employed to select signal and idler photons having the same polarization with the pump so that the SRS photons can be further suppressed [41]. The dual-band bandpass filter F_3, which is realized by cascading two coarse wavelength division multiplexing filters and a programmable optical filter (POF, model: Finisar Waveshaper 4000S), is used to select the signal and idler photons. By using the POF, the central wavelength and bandwidth of the signal and idler passbands of F_3 can be flexibly adjusted. The pump-rejection ratio provided by F_3 is in

Optics EXPRESS

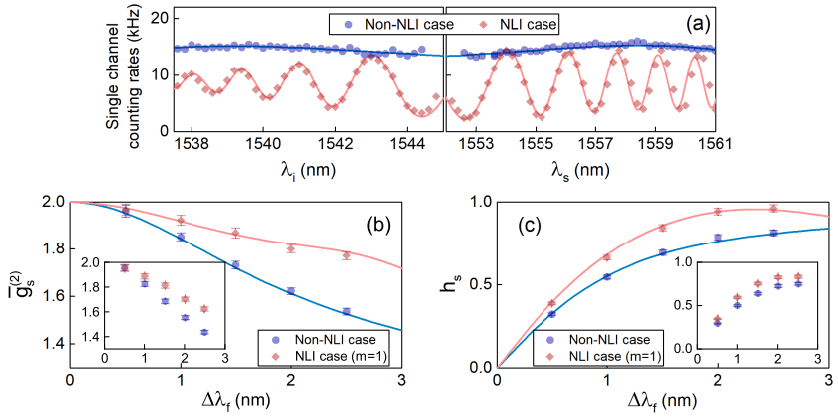

Fig. 4. (a) Measured marginal intensity distributions of signal (λ_s) and idler (λ_i) photons. The main plots of (b) and (c) are the corrected measurement results of intensity correlation function $\bar{g}_s^{(2)}$ and heralding efficiency h_s of signal photons as a function of filter bandwidth $\Delta\lambda_f$. The insets of (b) and (c) are the corresponding raw data. The diamonds and circles represent measured results for the NLI and non-NLI cases, respectively, while the curves are simulation results.

excess of 120 dB when the detuning between signal/idler and pump photons is greater than 4 nm, so photon pairs can be reliably measured by using single photon detectors (SPDs).

The signal and idler photons are then detected by SPD1 and SPD2, respectively. The SPDs are operated at gated Geiger mode with a gate repetition rate of 6.8 MHz. The detection efficiencies of SPD1 and SPD2 are about 12.5% and 15%, respectively. The overall detection efficiencies for the signal and idler photons (including insertion loss of F_3) are $\eta_s \approx 2.7\%$ and $\eta_i \approx 3.3\%$, respectively (deduced from fitting).

We first measure the spectra of the signal and idler photons produced from NLI (i.e., the marginal intensity distributions). In this experiment, the average pump power P_a is fixed at 120 μW, and the bandwidths of both channels of filter F_3 are set to 0.2 nm. The results (solid diamonds) in Fig. 4(a) are obtained by recording the single channel counting rate for signal (idler) field as the central wavelength of the signal (idler) channel of F_3 is scanned from 1552 (1545) nm to 1561 (1536) nm with a step of 0.2 nm. As a comparison, we then repeat the spectral measurement for the non-NLI case by removing the SMF and connecting the two DSFs directly, and the results (solid circles) are shown in Fig. 4(a) as well. The fitting curves in Fig. 4(a) are obtained by using the same theoretical model as that employed in plotting Figs. 2(a) and 2(b). Two free-fitting parameters are used to reflect the detection efficiencies in signal and idler channels, respectively. Note that adjusting the two parameters can proportionally change the whole level of the curves, but does not change the periodic pattern. From Fig. 4(a), one sees the measured spectra of signal and idler photon pairs are in good agreement with the theoretical predictions.

Next, we characterize the modal purity and heralding efficiency of the photon pairs from the NLI. In the experiment, the average pump power P_a is about 83 μW, and the central wavelength of the signal (idler) channel of F_3 is fixed at 1554 (1543) nm, corresponding to the m=1 island of the JSF (see Fig. 2). The one-side-filtered intensity correlation function $\bar{g}_{s(i)}^{(2)}$ and heralding efficiency $h_{s(i)}$ are measured when the filter bandwidth $\Delta\lambda_f$ for both signal and idler channels is adjusted to 0.5, 1, 1.5, 2, and 2.5 nm, respectively.

During the measurement of $h_{s(i)}$, we record the single channel counting rates of SPD1 and SPD2, R_1 and R_2, as well as the total coincidence and accidental coincidence rates of both

SPDs. The total coincidence is the coincidence of photons from the same pump pulse, while the accidental coincidence is the coincidence of photons from the adjacent pump pulses. The true coincidence rate C_t can be obtained by subtracting the accidental coincidence from the total coincidence. We then deduce $h_{s(i)}$ using $h_{s(i)} = \frac{C_t}{R_{2(1)}\eta_{s(i)}}$. When $\bar{g}^{(2)}_{s(i)}$ is measured, we send the individual signal (idler) field to a beam splitter (BS), then feed its two outputs into two SPDs (see inset of Fig. 3) and record the coincidence rates. We deduce $\bar{g}^{(2)}_{s(i)}$ by calculating the ratio between the measured total coincidence and accidental coincidence rates.

Since the variation tends of $\bar{g}^{(2)}_s$ and h_s of the signal field are similar to those of $\bar{g}^{(2)}_i$ and h_i of the idler field, here we only present the results of $\bar{g}^{(2)}_s$ and h_s, as shown in Figs. 4(b) and 4(c), respectively. The measured raw data is shown in the insets of Figs. 4(b) and 4(c), which clearly demonstrates that the results of $\bar{g}^{(2)}_s$ and h_s for the NLI case are better than those for the non-NLI case. To verify the validity of the theory in section 2, we correct the raw data by excluding the influence of background noise photons contributed by SRS (see Appendix and [42] for details) The corrected data of the NLI case (solid diamonds) and non-NLI case (solid circles) are fitted by the curves, which are obtained by using the same theoretical model in plotting Figs. 2(c) and 2(d). There is no free-fitting parameter used in fitting $\bar{g}^{(2)}_s$, while two free-fitting parameters related to the detection efficiencies for the signal and idler photons ($\eta_s = 2.7\%$ and $\eta_i = 3.3\%$) are used in fitting h_s. One sees the experimental data agree with the theoretical expectations quite well. The results indicate that modal purity and heralding efficiency can be simultaneously improved by using the NLI. It is worth to pointing out that if the background noise of SRS was almost completely suppressed by cooling the fiber to about 4 K [43], the performance of our source should be characterized by the corrected data.

4. Discussion

Although our idea of modifying JSF with quantum interference is verified by the proof-of-principle experiment, the results in Figs. 2 and 4 are not ideal. ${\bar{g}^{(2)}}_{s,i}$ and h_s deviate from their desired values of ${\bar{g}^{(2)}}_{s,i} \to 2$ and $h_{s,i} \to 1$. This is because adjacent islands of JSF are not separated enough from each other and there is overlap between them. To make the islands well separated, we need to finely control the phase by upgrading the crude phase control unit of DM. One solution is to replace the SMF with a programmable optical filter [44], with a large insertion loss though, to achieve arbitrary state engineering [32]. The other solution, which is more economic and practical, is to use a multi-stage NLI having high transmission efficiency.

As shown in Fig. 5(a), an N-stage NLI consists of N pieces of NMs and $N-1$ pieces of DMs. Assuming all the NMs and DMs are identical, the JSF is modified as

$$F^{(N)}_{NLI}(\omega_s, \omega_i) = F_{NM}(\omega_s, \omega_i)H(\theta) \tag{11}$$

with

$$H(\theta) = (\sin N\theta / \sin\theta)e^{j(N-1)\theta} \tag{12}$$

denoting the modulation function of multi-stage quantum interference, where θ is the same as in Eq. (8). From Eq. (12), we find the modulation function of two-photon state out of the multi-stage NLI is similar to the interference factor of multi-slit interferometer in classical optics.

To characterize this N-stage NLI, again we conduct simulations by employing DSFs (each of length 50 m) and SMFs (each of length 7 m) as the NMs and DMs, respectively. The contour plots of JSF $F^{(N)}_{NLI}(\omega_s, \omega_i)$ for $N = 3$, 4, and 5 are shown in Fig. 5(b). One sees that the separation between two adjacent islands is farther apart as N increases and the shapes also vary among islands with only one as the most factorable (rounded) for a specific N. Accordingly, the visibility of the interference pattern in marginal intensity distribution for signal field (see Fig. 5(b)) increases with N. The modal purity ($\bar{g}^{(2)}_s$) and heralding efficiency (h_s), corresponding

Optics EXPRESS

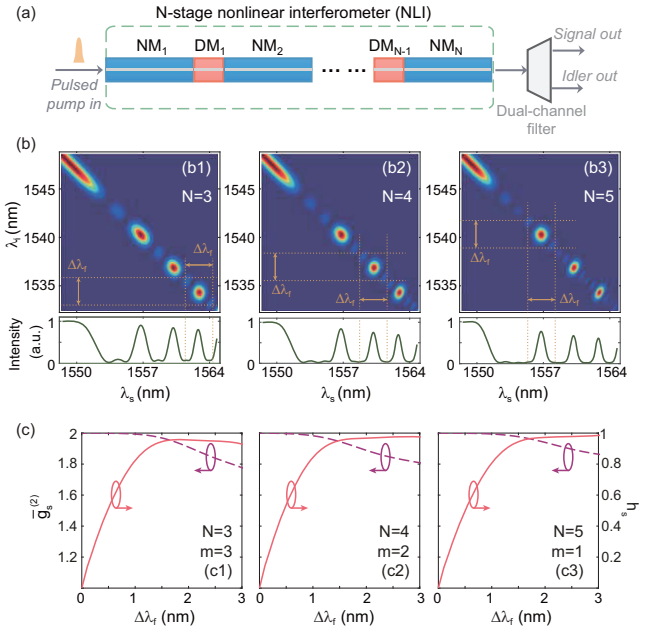

Fig. 5. (a) Schematic of N-stage nonlinear interferometer (NLI) with N pieces of nonlinear media (NMs) and $N-1$ pieces of linear dispersive media (DMs). (b) Contour plots of JSF and marginal intensity distribution in signal field for N-stage NLIs with DSFs and SMFs as the NMs and DMs, respectively. (b1)-(b3) are results for N=3, 4, and 5, respectively. (c) Calculated intensity correlation function $\bar{g}_s^{(2)}$ and heralding efficiency h_s as a function of filter bandwidth $\Delta\lambda_f$ for the most factorable islands in (b1)-(b3).

to the most factorable islands of $m = 3$, 2 and 1 for NLI with $N = 3$, 4, and 5, respectively, are plotted as a function of the filter bandwidth $\Delta\lambda_f$ in Fig. 5(c). Progressive improvement toward the ideal case of $\bar{g}_s^{(2)} = 2$ and $h_s = 1$ can be seen as N increases.

We note that different from the active filtering function in generating photon pairs from an optical parametric oscillator [45], which is an overall result of the resonant cavity, in the proposed N-stage NLI, each intermediate stage can be separated. Figure 5 shows that an N-stage NLI only has one island which corresponds to the most factorable JSF. However, we can make full use of the multiple stages by successively carving out the factorable islands, which can be realized by inserting proper dual-channel filters having reflection ports [32]. For example, for the case depicted in Fig. 5(b), we can insert a dual-channel filter after the 3rd NM (DSF) to carve out the $m = 3$ island and feed the reflect port of the filter to the next stage, then, use another dual-channel filter after the 4th NM (DSF) to obtain the $m = 2$ island. In this way, a multi-channel source of photon pairs with high purity and efficiency can be realized and can be further used to obtain multi-photon entanglement in multi-dimensions or multi-channel single photon source [46,47].

The JSA from a multi-stage NLI might be influenced by the length difference of different segments of nonlinear/dispersive media. Because the modulation term $H(\theta)$ in Eq. (11) is mainly determined by the dispersive media, the influence of length difference of dispersive media is far more crucial than that of nonlinear media. Actually, one important reason for using optical fibers in our schemes is that the length of fiber can be easily and accurately prepared. In practice, by using time-of-flight measurement and precise fiber-splicing, the length fluctuation of different dispersive fibers can be kept less than 0.1%. According to our simulation, this 0.1% fluctuation in length of dispersive fibers has subtle influence on the final JSF of a four-stage NLI, e.g., the

Optics EXPRESS

central wavelength of the island fluctuates less than 0.01 nm.

In fact, the idea of multi-stage NLI was previously proposed by U'Ren et al in the form of $\chi^{(2)}$-crystal sequence with intermediate birefringent spacers [31]. They also derived Eq. (11). As a comparison, however, our fiber-based nonlinear interferometers are much easier to realize and control. Moreover, we have the additional option of having multi-stage outputs by making use of the full spectrum satisfying phase matching condition of parametric process [32].

5. Conclusion

In summary, we propose a novel interferometric method to engineer the joint spectral function of a two-photon state generated from pulse pumped spontaneous parametric emission. As a proof-of principle demonstration, we successfully modify an originally un-factorized JSF from SFWM in one piece of dispersion shifted fiber to a nearly factorized JSF by using a two-stage NLI formed by two identical dispersion shifted fibers with a standard single mode fiber in between. Both the modal purity and heralding efficiency of photon pairs can be simultaneously improved without affecting the phase matching condition of SFWM.

The underlying physics of reshaping JSF is the interference fringe of photon pairs created by multi-stage NLI. By using the active filter effect of interference, the JSF of two-photon state in single piece nonlinear medium is divided into islands, which are separated from or orthogonal to each other and can be viewed as an individual JSF of two-photon state. The shape of each island and the distance between two adjacent islands can be flexibly adjusted by changing the length of linear dispersion medium and the stage number of the NLI. Therefore, the interferometric method is versatile and precise, arbitrary engineering in the production of entangled photon pairs can be easily realized. We believe the NLI can be used to generate various kinds of entangled states, such as spectrally uncorrelated polarization entangled photon pairs [28], multi-photon entanglement [11], and high-dimensional entangled state in multi-wavelength channels, etc. [46, 47]. Moreover, we think the NLI can be used for studying continuous variable quantum states with different temporal mode properties [48–50] when the parametric process of NLI is operated in high gain regime.

Appendix

Correction of data due to spontaneous Raman scattering (SRS)

The generation of correlated photon pairs through spontaneous four wave mixing (SFWM) in optical fiber is inevitably accompanied by the production of background noise originated from SRS, so the measured data should be corrected by subtracting the noise photons contributed by SRS.

The correction of collection efficiency $h_{s(i)}$ is straightforward. Since noise photons from SRS have no contribution to the true coincidence counts C_t, there is no need to correct C_t. For the photon counting rates $R_{1(2)}$ in individual signal (idler) channel, we measure $R_{1(2)}$ as a function of average pump power P_a and then fit the measured data with a second-order polynomial $R_{1(2)} = s_1 P_a + s_2 P_a^2$, where s_1 and s_2 are the fitting parameters. The linear and quadratic terms, $s_1 P_a$ and $s_2 P_a^2$, are respectively proportional to the intensities of SRS and SFWM [41]. By subtracting the portion of SRS photons from the raw data, we can correct $R_{1(2)}$ and then calculate the collection efficiency. For example, Fig. 6 shows the measured single channel counting rate of the idler photons in the NLI case. In this measurement, the common filter bandwidth is $\Delta\lambda_f$=2.5 nm. The solid curve is the fitting polynomial with the dash-dotted and dashed curves being the linear and quadratic terms, respectively.

For the intensity correlation measurement in the signal (idler) channel $\bar{g}^{(2)}_{s(i)}$, the influence of background noise cannot be directly subtracted due to the two-photon interference between two independent thermal fields. The signal (idler) photons, originated from both SFWM and SRS,

Optics EXPRESS

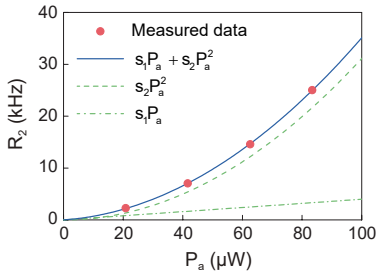

Fig. 6. Measured photon counting rate in individual idler channel R_2 as a function of average pump power P_a. The solid curve is the fitting polynomial $R_2 = s_1 P_a + s_2 P_a^2$ with s_1=39.8 and s_2=3.11. The dash-dotted and dashed curves are the linear and quadratic terms, respectively.

are in thermal state. In a recent paper [42], we have studied the two-photon interference effect of an interference field formed by mixing two thermal fields. Our investigation indicates that the measured raw data of $\bar{g}^{(2)}_{s(i)}$ is always less than the intensity correlation of signal (idler) photons generated from SFWM only. The amount of drop not only depends on the relative strength between SFWM photons and SRS photons (deduced from the measurement similar to Fig. 6), but relates to spectral properties of the two thermal fields. Hence, we also characterize the spectral property of SRS photons by measuring its intensity correlation function when the filter bandwidth $\Delta\lambda_f$ takes different values. This is done by selecting the SRS photons cross-polarized with SFWM photons [41] and fulfilling the $g^{(2)}$ measurement. Since the mode of signal photons originated from SFWM in NLI is very close to single-mode, we evaluate the factor $\mathcal{V}$ as the ratio between the bandwidths of SFWM photons and SRS photons, to describe the mode overlapping of two thermal fields. Finally, by substituting the raw data of $\bar{g}^{(2)}_{s(i)}$, the deduced relative strength of two thermal fields, and the evaluated value of $\mathcal{V}$ into Eq. (25) in [42], we obtain the corrected $\bar{g}^{(2)}_{s(i)}$ for the photons contributed by SFWM.

Funding

National Natural Science Foundation of China (11527808, 91736105, 11874279); National Key Research and Development Program of China (2016YFA0301403); US National Science Foundation (1806425); Science and Technology Program of Tianjin (18ZXZNGX00210).

References

1. D. M. Greenberger, M. A. Horne, and A. Zeilinger, *Going Beyond Bell's Theorem* (Springer, 1989), pp. 69–72.
2. M. Genovese, "Research on hidden variable theories: A review of recent progresses," Phys. Rep. **413**, 319–396 (2005).
3. D. Bouwmeester, A. K. Ekert, and A. Zeilinger, eds., *The Physics of Quantum Information* (Springer-Verlag, 2000).
4. J. L. O'Brien, A. Furusawa, and J. Vuckovic, "Photonic quantum technologies," Nat. Photonics **3**, 687–695 (2009).
5. S. Debnath, N. M. Linke, C. Figgatt, K. A. Landsman, K. Wright, and C. Monroe, "Demonstration of a small programmable quantum computer with atomic qubits," Nature **536**, 63–66 (2016).
6. J. Kelly, R. Barends, A. G. Fowler, A. Megrant, E. Jeffrey, T. C. White, D. Sank, J. Y. Mutus, B. Campbell, Y. Chen, Z. Chen, B. Chiaro, A. Dunsworth, I. C. Hoi, C. Neill, P. J. J. O'Malley, C. Quintana, P. Roushan, A. Vainsencher, J. Wenner, A. N. Cleland, and J. M. Martinis, "State preservation by repetitive error detection in a superconducting quantum circuit," Nature **519**, 66–69 (2015).
7. D. Bouwmeester, J. Pan, M. Klaus, E. Manfred, W. Harald, and Z. Anton, "Experimental quantum teleportation," Nature **403**, 575–579 (1997).
8. H. Wang, Y. He, Y.-H. Li, Z.-E. Su, B. Li, H.-L. Huang, X. Ding, M.-C. Chen, C. Liu, J. Qin, J.-P. Li, Y.-M. He, C. Schneider, M. Kamp, C.-Z. Peng, S. Höfling, C.-Y. Lu, and J.-W. Pan, "High-efficiency multiphoton boson sampling," Nat. Photonics **11**, 361–365 (2017).

Optics EXPRESS

9. Z.-E. Su, Y. Li, P. P. Rohde, H.-L. Huang, X.-L. Wang, L. Li, N.-L. Liu, J. P. Dowling, C.-Y. Lu, and J.-W. Pan, "Multiphoton interference in quantum fourier transform circuits and applications to quantum metrology," Phys. Rev. Lett. **119**, 080502 (2017).
10. P. Kok, W. J. Munro, K. Nemoto, T. C. Ralph, J. P. Dowling, and G. J. Milburn, "Linear optical quantum computing with photonic qubits," Rev. Mod. Phys. **79**, 135–174 (2007).
11. X.-C. Yao, T.-X. Wang, P. Xu, H. Lu, G.-S. Pan, X.-H. Bao, C.-Z. Peng, C.-Y. Lu, Y.-A. Chen, and J.-W. Pan, "Observation of eight-photon entanglement," Nat. Photonics **6**, 225–228 (2012).
12. C. Santori, D. Fattal, J. Vuckovic, G. S. Solomon, and Y. Yamamoto, "Indistinguishable photons from a single-photon device," Nature **419**, 594–597 (2002).
13. X. Ding, Y. He, Z.-C. Duan, N. Gregersen, M.-C. Chen, S. Unsleber, S. Maier, C. Schneider, M. Kamp, S. Höfling, C.-Y. Lu, and J.-W. Pan, "On-demand single photons with high extraction efficiency and near-unity indistinguishability from a resonantly driven quantum dot in a micropillar," Phys. Rev. Lett. **116**, 020401 (2016).
14. C. K. Hong and L. Mandel, "Experimental realization of a localized one-photon state," Phys. Rev. Lett. **56**, 58–60 (1986).
15. W. P. Grice and I. A. Walmsley, "Spectral information and distinguishability in type-ii down-conversion with a broadband pump," Phys. Rev. A **56**, 1627 (1997).
16. W. P. Grice, A. B. U'Ren, and I. A. Walmsley, "Eliminating frequency and space-time correlations in multiphoton states," Phys. Rev. A **64**, 063815 (2001).
17. P. Qian, Z. Gu, R. Cao, R. Wen, Z. Y. Ou, J. F. Chen, and W. Zhang, "Temporal purity and quantum interference of single photons from two independent cold atomic ensembles," Phys. Rev. Lett. **117**, 013602 (2016).
18. P. J. Mosley, J. S. Lundeen, B. J. Smith, P. Wasylczyk, A. B. U'Ren, C. Silberhorn, and I. A. Walmsley, "Heralded generation of ultrafast single photons in pure quantum states," Phys. Rev. Lett. **100**, 133601 (2008).
19. Z. Y. Ou, J. K. Rhee, and L. J. Wang, "Photon bunching and multiphoton interference in parametric down-conversion," Phys. Rev. A **60**, 593–604 (1999).
20. J. G. Rarity, "Interference of single photons from separate sourcesa," Annals New York Acad. Sci. **755**, 624–631 (1995).
21. S. Castelletto, I. P. Degiovanni, V. Schettini, and A. Migdall, "Spatial and spectral mode selection of heralded single photons from pulsed parametric down-conversion," Opt. Express **13**, 6709–6722 (2005).
22. M. G. Raymer, J. Noh, K. Banaszek, and I. A. Walmsley, "Pure-state single-photon wave-packet generation by parametric down-conversion in a distributed microcavity," Phys. Rev. A **72**, 023825 (2005).
23. K. Garay-Palmett, H. J. McGuinness, O. Cohen, J. S. Lundeen, R. Rangel-Rojo, A. B. U'Ren, M. G. Raymer, C. J. McKinstrie, S. Radic, and I. A. Walmsley, "Photon pair-state preparation with tailored spectral properties by spontaneous four-wave mixing in photonic-crystal fiber," Opt. Express **15**, 14870–14886 (2007).
24. O. Cohen, J. S. Lundeen, B. J. Smith, G. Puentes, P. J. Mosley, and I. A. Walmsley, "Tailored photon-pair generation in optical fibers," Phys. Rev. Lett. **102**, 123603 (2009).
25. B. J. Smith, P. Mahou, O. Cohen, J. S. Lundeen, and I. A. Walmsley, "Photon pair generation in birefringent optical fibers," Opt. Express **17**, 23589–23602 (2009).
26. L. Cui, X. Li, and N. Zhao, "Minimizing the frequency correlation of photon pairs in photonic crystal fibers," New J. Phys. **14**, 123001 (2012).
27. B. Fang, O. Cohen, J. B. Moreno, and V. O. Lorenz, "State engineering of photon pairs produced through dual-pump spontaneous four-wave mixing," Opt. Express **21**, 2707–2717 (2013).
28. P. G. Evans, R. S. Bennink, W. P. Grice, T. S. Humble, and J. Schaake, "Bright source of spectrally uncorrelated polarization-entangled photons with nearly single-mode emission," Phys. Rev. Lett. **105**, 253601 (2010).
29. A. M. Branczyk, A. Fedrizzi, T. M. Stace, T. C. Ralph, and A. G. White, "Engineered optical nonlinearity for quantum light sources," Opt. Express **19**, 55–65 (2011).
30. M. V. Chekhova and Z. Y. Ou, "Nonlinear interferometers in quantum optics," Adv. Opt. Photonics **8**, 104–155 (2016).
31. A. B. U'Ren, C. Silberhorn, R. Erdmann, K. Banaszek, W. P. Grice, I. A. Walmsley, and M. G. Raymer, "Generation of pure-state single-photon wavepackets by conditional preparation based on spontaneous parametric downconversion," Laser Phys. **15**, 146 (2005).
32. J. Su, L. Cui, J. Li, Y. Liu, X. Li, and Z. Y. Ou, "Quantum state engineering by nonlinear quantum interference," arXiv:1811.07646 (2018).
33. B. Yurke, S. L. McCall, and J. R. Klauder, "Su(2) and su(1,1) interferometers," Phys. Rev. A **33**, 4033–4054 (1986).
34. F. Hudelist, J. Kong, C. Liu, J. Jing, Z. Y. Ou, and W. Zhang, "Quantum metrology with parametric amplifier-based photon correlation interferometers," Nat. Commun. **5**, 3049 (2014).
35. G. B. Lemos, V. Borish, G. D. Cole, S. Ramelow, R. Lapkiewicz, and A. Zeilinger, "Quantum imaging with undetected photons," Nature **512**, 409–412 (2014).
36. D. A. Kalashnikov, A. V. Paterova, S. P. Kulik, and L. A. Krivitsky, "Infrared spectroscopy with visible light," Nat. Photonics **10**, 98–101 (2016).
37. A. B. U'Ren, R. K. Erdmann, M. de la Cruz-Gutierrez, and I. A. Walmsley, "Generation of two-photon states with an arbitrary degree of entanglement via nonlinear crystal superlattices," Phys. Rev. Lett. **97**, 223602 (2006).
38. C. K. Law, I. A. Walmsley, and J. H. Eberly, "Continuous frequency entanglement: effective finite hilbert space and entropy control," Phys. Rev. Lett. **84**, 5304–5307 (2000).

Optics EXPRESS

39. L. Yang, X. Ma, X. Guo, L. Cui, and X. Li, "Characterization of a fiber-based source of heralded single photons," Phys. Rev. A **83**, 053843 (2011).
40. N. Liu, Y. Liu, X. Guo, L. Yang, X. Li, and Z. Y. Ou, "Approaching single temporal mode operation in twin beams generated by pulse pumped high gain spontaneous four wave mixing," Opt. Express **24**, 1096–108 (2016).
41. X. Li, P. Voss, J. Chen, K. Lee, and P. Kumar, "Measurement of co- and cross-polarized raman spectra in silica fiber for small detunings," Opt. Express **13**, 2236–2244 (2005).
42. J. Su, J. Li, L. Cui, X. Li, and Z. Y. Ou, "Interference between two independent multi-temporal-mode thermal fields," Phys. Rev. A **99**, 013838 (2019).
43. S. D. Dyer, M. J. Stevens, B. Baek, and S. W. Nam, "High-efficiency, ultra low-noise all-fiber photon-pair source," Opt. Express **16**, 9966–9977 (2008).
44. A. M. Weiner, "Femtosecond pulse shaping using spatial light modulators," Rev. Sci. Instruments **71**, 1929–1960 (2000).
45. Z. Y. Ou and Y. J. Lu, "Cavity enhanced spontaneous parametric down-conversion for the prolongation of correlation time between conjugate photons," Phys. Rev. Lett. **83**, 2556–2559 (1999).
46. M. Huber and J. de Vicente, "Structure of multidimensional entanglement in multipartite systems," Phys. Rev. Lett. **110**, 030501 (2013).
47. M. Kues, C. Reimer, P. Roztocki, L. R. Cortes, S. Sciara, B. Wetzel, Y. Zhang, A. Cino, S. T. Chu, B. E. Little, D. J. Moss, L. Caspani, J. Azana, and R. Morandotti, "On-chip generation of high-dimensional entangled quantum states and their coherent control," Nature **546**, 622–626 (2017).
48. A. Eckstein, A. Christ, P. J. Mosley, and C. Silberhorn, "Highly efficient single-pass source of pulsed single-mode twin beams of light," Phys. Rev. Lett. **106**, 013603 (2011).
49. J. Roslund, R. M. de Araujo, S. Jiang, C. Fabre, and N. Treps, "Wavelength-multiplexed quantum networks with ultrafast frequency combs," Nat. Photonics **8**, 109–112 (2013).
50. B. Brecht, D. V. Reddy, C. Silberhorn, and M. G. Raymer, "Photon temporal modes: A complete framework for quantum information science," Phys. Rev. X **5**, 041017 (2015).